On the observed changes in upper stratospheric and mesospheric temperatures from UARS HALOE

by E. Remsberg[1]

[1]Science Directorate, NASA Langley Research Ctr., Hampton, VA, USA

E. E. Remsberg, Science Directorate, Mail Stop 401B, 21 Langley Blvd., NASA Langley Research Ctr., Hampton, VA, USA 23681-2199. (e-mail: Ellis.E.Remsberg@nasa.gov)

Abstract. Temperature versus pressure or T(p) time series from the Halogen Occultation Experiment (HALOE) on the Upper Atmosphere Research Satellite (UARS) have been extended and re-analyzed for the period of 1991-2005 and for the upper stratosphere and mesosphere in 10-degree wide latitude zones from 60S to 60N. Even though sampling from a solar occultation experiment is somewhat limited, it is shown to be quite adequate for developing both the seasonal and longer-term variations in T(p). Multiple linear regression (MLR) techniques were used in the re-analyses for the seasonal and the significant interannual, solar cycle (SC-like or decadal-scale), and linear trend terms. A simple SC-like term of 11-yr period was fitted to the time series residuals after accounting for the seasonal and interannual terms. Highly significant SC-like responses were found for both the upper mesosphere and the upper stratosphere. The phases of these SC-like terms were checked for their continuity with latitude and pressure-altitude, and in almost all cases they are directly in-phase with that of standard proxies for the solar flux variations. The analyzed, max minus min, responses at low latitudes are of order 1 K, while at middle latitudes they are as large as 3 K in the upper mesosphere. Highly significant, linear cooling trends were found at middle latitudes of the middle to upper mesosphere (about -2 K/decade), at tropical latitudes of the middle mesosphere (about -1 K/decade), and at 2 hPa (or order -1 K/decade).

Keywords. Atmospheric composition and structure (pressure, density and temperature), Meteorology and atmospheric dynamics (climatology; middle atmosphere dynamics)

1 Introduction

Efforts to understand the seasonal and longer-term variations of the temperature distribution of the mesosphere (Beig et al., 2003; Laštovička, et al., 2006) have been ongoing for three to four decades using ground-based lidar and in situ rocket measurement techniques, respectively (see e.g., Keckhut et al., 2005; Kubicki et al., 2006). Although those techniques are providing good quality time series of temperature data above geophysical observing stations, it has been difficult for analysts to resolve the atmospheric temperature response to the forcing of the 11-yr solar cycle and then the underlying trends due to changes in the so-called "greenhouse gases" using datasets from fixed, local sites (e.g., Hampson et al., 2006). It has also been difficult to use station data to verify model simulations of changes in the zonal mean temperature (e.g., Akmaev et al., 2006; Kodera and Kuroda, 2002; Gruzdev and Brasseur, 2005). Satellite measurement techniques are providing datasets on the seasonal and interannual variations of the zonal mean mesospheric temperature (e.g., Fleming et al., 1990; Shepherd et al., 2005), but up until recently they have been limited to time spans that are considerably shorter than a solar cycle.

Remsberg (2006) reports on findings from time series of temperature versus pressure (or T(p)) based on 95,900 sunrise (SR) plus sunset (SS) measured profiles from the HALogen Occultation Experiment (HALOE) satellite experiment (Russell et al., 1993). This 14-year (1991-2005) dataset on T(p) extends for more than one complete solar cycle, making it possible to separate any long-term trend from the effects of the solar

forcing. HALOE obtained an exo-atmospheric look at the Sun as part of the signal normalization procedures for each of its measured atmospheric profiles. In addition, in-orbit calibration measurements of the performance characteristics of the HALOE instrument were obtained throughout its mission lifetime. No significant changes have been found that affect the fidelity of the time series of T(p) from HALOE (Gordley et al., 2006).

The HALOE profiles of T(p) are based strictly on retrievals of its 2.8-μm CO_2 channel transmission profiles above about the 3-hPa altitude. At the 5-hPa altitude and below, the T(p) information is entirely based on the analyses from the NOAA Climate Prediction Center (CPC). Above the 0.007-hPa altitude there is a tie-in to the MSIS-90 climatology. Vertical resolution of the individual retrieved T(p) profiles is of order 3.5 km. Time series of zonal average T(p) data are generated from the profiles and analyzed for 13 latitude zones from 60S to 60N and for 16 pressure levels from 2 hPa (near 43 km) to 0.007 hPa (near 82 km)—a total of 208 separate time series for this analysis. The time series analyses herein have been conducted for constant pressure levels, rather than for constant altitude levels, in order to make it easier to analyze for the vertically-local effects of the seasonal variations and to delineate the diabatic forcings for the T(p) profiles due to the solar flux and to the radiative cooling from CO_2.

This paper is complementary to and extends the material of Remsberg (2006). Section 2 describes briefly the approach that was taken for the analyses. Section 3 contains information on the amplitudes and phases of the seasonal terms and on the annual

temperature distributions at 20N and 40N for comparisons with those from ground-based measurements. The zonal mean distributions of amplitudes of the interannual terms are shown and compared with those reported from other satellite datasets. Section 4 then reviews the findings from HALOE for the SC-like and the trend terms for comparisons with model results and with other datasets. Section 5 contains some discussion of the findings in Section 4 and also of those regions where the phase or magnitude of the 11-yr term disagrees with that for a direct, solar forcing mechanism.

2 Data Analysis Approach

The limb occultation measurements of the Sun by HALOE occur at two local times (SR and SS). Remsberg et al. (2001), Remsberg and Deaver (2005), and Remsberg (2006) have analyzed the time series of SR plus SS ozone and/or temperature data at latitudes and selected pressure-altitudes. SR and SS measurements occur, on average, about every 25 days for a given 10-degree wide latitude zone. Locations of the SR and SS tangent points are shown in Remsberg et al. (2001) for each day of 1995. A 25-dy sampling frequency is quite adequate for characterizing even the shorter-period, semi-annual variations in T(p), which are especially significant for the mid mesosphere at low latitudes. Figure 1 is an example of one such time series for the Equator and the 0.15-hPa level of the mid mesosphere (at about 62 km). The oscillating curve is the multiple linear regression (MLR) fit to the time series of about 200 points and is based on a model that includes annual (AO), semi-annual (SAO), sub-biennial (640-dy or IA), and 4015-dy (11-yr or SC) terms. The horizontal line is the constant term from the model. There is a clear SS minus SR mean bias of 6.9 K in the data at this level and latitude that is due to the

effects of tides to first order. Although the MLR model fit for the seasonal terms in Figure 1 is reasonable, its short-period (or noise-like) residuals are considerable and tend to limit the accuracy of the fit for the smaller-amplitude, longer-period terms and the trend term. Therefore, Remsberg (2006) adjusted the SR and SS points by half their average difference and then re-combined them as shown in Figure 2. As a result, he obtained better continuity for the time series points and an improved fit for all the MLR model terms. The residuals for the model fit of Figure 2 are shown in Figure 3. The solid horizontal line is a linear fit to the residuals, and it indicates no underlying trend.

The points in Figures 1 and 2 consist generally of alternating occurrences for SR and SS at a zone of latitude. The combined time series of Figure 1 has a lag-1 autocorrelation coefficient that is highly negative (AR1 = -0.49). After making the SR/SS adjustment AR1 becomes weakly positive (AR1 = 0.16) for the series of Figure 2, indicating some point-to-point memory for the non-diurnal, zonal mean state of the tropical mid-mesosphere. Therefore, the analysis sequence is: (1) obtain an initial fit to the adjusted time series, (2) determinate its AR1 coefficient, (3) transform the terms of the model to account for that memory, and (4) then perform another fit using those transformed terms. As customary, the final residuals of Figure 3 were checked for any significant structure.

Because the seasonal (AO and SAO) cycles in the time series generally have much larger amplitudes than those of the longer period terms (e.g., QBO-like, sub-biennial, and solar cycle (or SC-like)), it is important to account for those seasonal variations with very good accuracy. After Remsberg (2006) fit the data for the seasonal terms he Fourier-analyzed

the residuals for any longer-period structure. He found 853-dy (or QBO-like) and 640-dy (or sub-biennial) cycles in the residuals for many latitudes and pressure altitudes. Where those terms were highly significant, he added them to his MLR models. Finally, he included a sinusoidal SC-like term having a 4015-dy (11-yr) period and/or a trend term to the MLR models of each latitude and pressure-level. The fit to the data was the basis for the determination of the phase of the 11-yr term. Wherever it was nearly in-phase with a solar uv-flux proxy (11-yr maximum occurring within +/-2 yr of uv-flux maximum), he assumed that this term was SC-like and due to the expected, direct solar-flux forcing mechanism. If the 11-yr term had amplitude that was considerably larger than expected and/or was not in-phase with the flux, he assumed that there was an additional, perhaps decadal-scale, dynamical forcing mechanism that was responsible.

3 Seasonal and Interannual Terms

Remsberg (2006) contains tabulations of the amplitudes and phases of the semiannual (SAO) and annual (AO) terms, plus zonal mean cross section plots of their amplitudes, from 60S to 60N and from 0.007 to 2 hPa. His analyses for the seasonal, interannual, and annual average terms are extended here to include values at 3 and 5 hPa, as shown in Table 1. Plots of the amplitudes and phases of the SAO terms are given in Figures 4 and 5, respectively, for the range of pressure-altitudes of the upper stratosphere and mesosphere. Analogous plots for the AO terms are shown in Figures 6 and 7. The distribution of the annual average temperature from HALOE is shown in Figure 8. Variations of the annual average and seasonal terms are similar to those reported previously from temperature climatologies obtained with other satellite datasets [e.g.,

Barnett et al., 1985; Shepherd et al., 2004; Huang et al., 2006]. Some differences are expected depending on whether the comparison climatologies are referenced against pressure or altitude. The climatology herein is somewhat unique because the HALOE SR and SS temperatures have been adjusted for the average effects of tides. However, there may be residual biases for the AO amplitudes, and especially for the SAO amplitudes at low latitudes, because this first order adjustment for the combined HALOE time series does not consider seasonal variations of the tides (see e.g., Huang et al., 2006). The seasonal and annual mean temperatures from these HALOE analyses are also essentially free of the small, but significant interannual and solar cycle terms because those terms were accounted for as part of the MLR model fit to the time series.

The annual average and seasonal values reported in Remsberg (2006), as extended to 5 hPa herein, can be used to generate the seasonal variation of T(p) at a given latitude. As examples, Figures 9 and 10 show the seasonal variations for T(p) at 20N and 40N, respectively. They compare very favorably with the seasonal variations of temperature versus altitude (or T(z)) obtained for stations at 19.5N, 204E and 44N, 6E using ground-based lidar instruments (see Plate 1 in Leblanc et al., 1998). The zonal mean HALOE results for 40N do not show the same amount of warming in the mid mesosphere in November as the lidar station data, due to longitudinal variations of the temperature for the winter hemisphere. Seasonal variations can also be generated from the HALOE data for the higher latitudes of 50 and 60 degrees because HALOE sampled those latitudes often enough to define the dominant AO term, at least.

Remsberg (2006) contains a tabulation of the amplitudes of the two primary interannual terms having periods of 853 days (28-month, quasi-biennial or QBO) and 640 days (21-month, sub-biennial or IA), respectively. He determined those dominant periods from a Fourier analysis of the time series residuals after accounting for the seasonal terms. Although he was unable to resolve significant interannual terms for every latitude and pressure-altitude, terms were found at most of the zonal mean grid locations. Interpolations were applied to fill in the missing parts of the grid and to generate plots.

Figure 11 shows the distribution of the amplitudes for the QBO-like terms. They are small (of order 0.9 K or less) throughout the tropical and subtropical upper stratosphere and mesosphere. Somewhat larger amplitudes occur at about 0.01 hPa at the Equator. Larger amplitudes (0.9 K to 1.5 K) are also present at 40 to 50 degrees of latitude in both hemispheres. It is important to remember that the amplitudes of the QBO terms from HALOE are obtained with respect to pressure (not altitude) surfaces, and that the QBO is primarily due to dynamical forcings. Therefore, any atmospheric temperature response should be somewhat adiabatic and not so apparent in pressure coordinates. With that in mind, the QBO amplitudes of Figure 11 are compared with those obtained in altitude coordinates from the SABER dataset by Huang et al. (2006, their Figure 2). Both analyses indicate significant amplitudes at Equatorial latitudes of the upper mesosphere, although the HALOE results do not show the maximum at 70 km that was obtained for SABER by Huang et al. (2006). HALOE also shows a maximum in the upper stratosphere, although its amplitude is about half that obtained from the SABER analyses. However, Huang et al. (2006) also show QBO analyses from the MLS dataset, but at

constant pressure levels. The QBO signal in the tropical upper stratosphere is much weaker from MLS and more in line with the present values from HALOE.

The pronounced QBO amplitudes at 40 to 50 degrees of latitude from HALOE agree qualitatively with those found from the SABER dataset by Huang et al. (2006). Still the amplitudes from HALOE are smaller, perhaps due to conducting the analyses at constant pressure rather than altitude levels. It is presumed that the smaller amplitudes from the HALOE dataset are related to the effects of the QBO forcing for the net, diabatic circulation.

The sub-biennial (IA or 640-dy) term arises due to interactions between the QBO cycle and the AO and SAO cycles. The distribution of amplitudes for this IA term is shown in Figure 12. Results do not extend to 3 and 5 hPa because IA terms were not significant at those pressures for most of the low latitudes. Maxima occur in Figure 12 at the Equator near 0.01 hPa and at 40 and 50 degrees near 0.1 hPa, and the IA term is highly significant in those regions. It is believed that the distribution of this term has not been resolved or reported for the mesosphere from any other satellite datasets. Nevertheless, it is very important to account for the structure from interannual terms, like the QBO and IA, before attempting to fit the time series with an 11-year solar cycle (or SC-like) term and/or a linear trend term.

4 Solar Cycle and Trend Terms

The findings for the seasonal and interannual terms of the preceding section are preliminary to the goal of analyzing the HALOE time series for its response to the solar cycle forcing and a long-term cooling trend due to the increasing amounts of the atmospheric "greenhouse gases". Remsberg (2006) successfully used the MLR technique to resolve an SC-like term by assuming that it had an 11-yr period but then allowing the fit to the residuals to determine its phase. He labeled his approach as "exploratory" because he wanted to consider other possible decadal-scale forcings for the temperature time series. Thus, instead of regressing directly against a standard solar flux proxy, he simply checked to see whether the phases of the SC-like terms that he found were within ±2 yr of January 1991 (or 2002). In general, the time span for maximum solar flux conditions is broad and extends for several years. Where that ±2 yr criterion was met, he applied a cosine weighting to the amplitudes based on the absolute time difference from a January 1991 SC maximum and then multiplied those adjusted amplitudes by two to obtain an estimate of "max minus min" SC temperature differences. Table 2 contains those differences; it has blank entries for those locations where the absolute phase differences were greater than 2 years. That circumstance occurred for a number of pressure levels at 60S and 60N and in the upper mesosphere at the Equator. Although significant 11-yr terms were found there, they were generally out-of-phase with the solar flux (see discussion in Section 5). Analyses were not conducted for the SC-like and trend terms at 3 and 5 hPa because of the close proximity of those levels with the mid stratospheric tie-in for the retrieved HALOE T(p) profiles to stratospheric analyses from NOAA-CPC. Thus, it is likely that any long-term changes at those two levels cannot be attributed entirely to the measurements from HALOE.

To enable one to judge more easily the variations for the direct solar response, the data in Table 2 were averaged for 5 latitude zones—50-60S, 20-40S, 10S-10N, 20-40N, and 50-60N. Vertical interpolations were applied to fill-in data gaps for several of the levels. The seasonal sampling from HALOE is marginal for the 50-60 latitude zones, so their SC-like terms are also less certain and have been given separately. The latitude ranges for the groupings are also different from those in Remsberg (2006), making it easier to compare with the SC responses near the stratopause from models. Results for all 5 zones are given in Table 3 and plotted in Figure 13. One can see that there is an in-phase, SC-like response that increases with latitude and with altitude away from the Equator. Results for the adjacent 20-40 and 50-60 zones are similar within a hemisphere, indicating that any effect of the reduced HALOE sampling for the higher latitude zones is not noticeable. The observed, max minus min, response for the tropical zone is of order 1 K, while at middle latitudes it becomes as large as 3 K in the upper mesosphere.

Most model simulations of the mesospheric T(p) response to a direct solar uv-flux forcing indicate weak increases with altitude and with latitude, at least for the winter hemisphere (e.g., Garcia et al., 1984; Huang and Brasseur, 1993; Shindell et al., 1999; Khosravi et al., 2002). At tropical latitudes the modeled responses have a minimum in the low to mid mesosphere but increase near the stratopause and in the uppermost mesosphere. Those results agree well with the ones from HALOE in Table 2. The analyzed, peak HALOE, max minus min, SC responses of 0.7 to 1.8 K near the tropical stratopause are related to the response of ozone to the uv-flux. They agree with the

recent analyses from the ERA-40 dataset (Crooks and Gray, 2005) and from the separate analyses of the HALOE data by Fadnavis and Beig (2006a). Those observed responses have also been modeled well (e.g., Hampson et al., 2005; Matthes et al., 2004). Thus, it is postulated that the larger than expected HALOE SC-like responses at mid to high latitudes of the upper mesosphere are associated with a decadal-scale, dynamical response that is also in-phase with the solar flux forcing but has not been represented well in models.

The MLR technique provides for the simultaneous fitting of polynominal terms to the HALOE time series, in addition to all the foregoing periodic terms. In particular, Remsberg (2006) found highly significant linear trends at a number of latitudes and pressure-altitudes from his analyses. Those results have been grouped and averaged into the 3 latitude zones of 30-40S, 20S-20N, and 30-40N for Table 4 and Figure 14. The confidence intervals for the terms have also been simply averaged within each zone for Table 4. It is noted that the linear trends were somewhat erratic and had large uncertainties at several levels of the higher latitude, 50-60 degree zones, most likely because the seasonal sampling was not good toward the end of the HALOE time series. Therefore, the high latitude trend results were excluded from Table 4.

Trends from near the stratopause through the lower mesosphere are fairly uniform with latitude and of order -0.5 to -1.0 K/decade. These cooling trends do not increase by much through the upper mesosphere at low latitudes. However, there is a clear increase in the trends for middle latitudes of both hemispheres to more than -2 K/decade, and those

values are highly significant. In the uppermost mesosphere the trends decrease to -0.5 K/decade at the northern middle latitudes. Simulations of the rate of cooling due to the increasing "greenhouse gases" are in general agreement with cooling rates of -0.5 to -1.0 K/decade for the mesosphere, particularly if the only gas that is changing is CO_2 (e.g., Akmaev et al., 2006). Clearly, there are other mechanisms contributing to the cooling trends from the HALOE data of the upper mesosphere at middle latitudes.

The enhanced cooling rates of -0.8 to -1.3 K/decade at 2 hPa of the upper stratosphere are highly significant. They agree with those reported by Fadnavis and Beig (2006b) for low latitudes. These cooling rates also are within the range of model results in Shine et al. (2003). Akmaev et al. (2006) calculated somewhat larger global cooling rates of about -2 K/decade near the stratopause. However, their results are for the period 1980-2000, when the decline in ozone (and the decline in its radiative heating) was contributing to their calculated net cooling. The HALOE measurements were taken when the decline of the ozone was slowing. Trends in upper stratospheric temperatures have not been reported from other datasets for comparisons with the specific period of HALOE—1991-2005.

5 **Discussion and Summary**

The findings herein represent new results for the SC-like and trend terms of T(p) since Beig et al. (2003), and in many respects there is good agreement with the results from models. However, the SC-like responses and trends from HALOE for the middle latitudes of the upper mesosphere are definitely larger than those from most models. This region is where planetary waves tend to break, particularly for the winter/spring period.

Gravity waves and tides also begin to break in the upper mesosphere, and it is a region of observed mesospheric inversion layers (MIL). The propagation of planetary waves to the mesosphere may be enhanced under solar maximum conditions, giving rise to an additional T(p) response that is in-phase with the solar cycle. For example, Kirkwood and Stebel (2003) report a decadal-scale correlation for the phase of the stationary planetary waves and their associated effects on the net circulation for the occurrence of noctilucent clouds (NLC) near the polar summer mesopause. It is reasonable to expect that such forcings could affect T(p) at middle latitudes of the upper mesosphere, as well.

There have been several recent modeling studies of a dynamical response to the solar cycle forcing that indicate a reinforcement of the normal radiative temperature response in the mesosphere at solar maximum (Kodera and Kuroda, 2002; Hampson et al., 2005). Koshravi et al. (2002) conducted 2-d model simulations to see whether they could produce a dynamically-induced temperature response to the solar flux forcing. They found significant, in-phase temperature responses to the SC of several K, particularly in the winter hemisphere of the upper mesosphere. Schmidt et al. (2006) also found SC-like responses of order 3 K near the mesopause from their 3-d model simulations, but weakening to less than 1 K below 75 km. Such a rapid decline toward lower altitudes is in reasonable accord with profiles of the SC-like response from HALOE for middle latitudes (Figure 13). There is also a decadal-scale, response in T(p) at 60 degrees latitude in the upper stratosphere to the middle mesosphere that is out-of-phase with the solar forcing (see Table 2 and also Remsberg (2006, Table 11)). It is speculated that this character is an indirect radiative and dynamical response to effects of the solar forcing at

adjacent altitudes and/or lower latitudes—perhaps in association with occurrences of the sudden stratospheric winter warming events.

Schmidt et al. (2006) found a significant cooling due to the increases in CO_2 that was pronounced for the middle latitudes of the winter hemisphere but weaker at low latitudes. Presumably, their annual average model results show a relatively smaller cooling at low latitudes as compared with middle latitudes—in qualitative agreement with the findings from HALOE in Figure 14. Gruzdev and Brasseur (2005) used an interactive 2-d model to investigate trends in T(p) due to increasing "greenhouse gases". Although their results were similar to those of Schmidt et al. (2006), they point out that there can also be long-term changes in T(p) due to the dynamics and the gravity wave activity that should be associated with the changes in the thermal structure from just radiative and chemical processes.

To summarize, 14-year time series of HALOE SR and SS T(p) data have been analyzed for their seasonal, interannual, SC-like, and trend terms from 60S to 60N and from 5 hPa to 0.007 hPa (but only from 2 to 0.007 hPa for the SC-like and trend terms). The seasonal and annual mean terms have reasonable amplitudes and phases and can be used to generate a seasonal, zonal average climatology for a given latitude zone. Two interannual terms (QBO-like and sub-biennial) are prominent at most of the latitudes and pressure-altitudes. Significant SC-like and trend terms were also found from the analyses at many, but not all locations. The SC-like terms are generally in-phase with the solar flux forcing and have amplitudes in the tropics that agree with most model results. There

is an increasing SC-like response from low to middle latitudes of the upper mesosphere that is presumed to be due to decadal-scale, dynamical processes that are also in-phase with the solar forcing. The cooling trends that have been resolved also agree with those from several radiative/dynamical models of the effects of the increasing amounts of atmospheric CO_2 in the mesosphere and upper stratosphere.

Acknowledgements. The author is grateful to have had the opportunity to present these findings at the 4th Workshop for the Climate and Weather of the Sun-Earth System (CAWSES) held in Sodankyla, Finland, in September 2006. He also expresses his appreciation to Jim Russell (HALOE—Principal Investigator) and to the members of the HALOE Project Team for producing and documenting its high quality dataset. The analyses herein were supported with funds for the UARS HALOE Project administered by Charley Jackman of NASA/GSFC and by Mike Kurylo of NASA/Hdqtrs.

References

Akmaev, R. A., V. I. Fomichev, and X. Zhu: Impact of middle-atmospheric composition changes on greenhouse cooling in the upper atmosphere, J. Atmos. Solar Terr. Phys., ?, doi:10.1016/j.jastp.2006.03.008, 2006.

Barnett, J. J., M. Corney, and K. Labitzke: Annual and semiannual cycles based on the middle atmosphere reference model in Section 2.2, in Handbook for Middle Atmosphere Program (MAP), vol. 16, K. Labitzke, J. J. Barnett, and B. Edwards, Eds., SCOSTEP Secretariat, U. of Illinois, Urbana, IL, 175-180, 1985.

Beig, G., P., P. Keckhut, R. P. Lowe, et al.: Review of mesospheric temperature trends, Rev. Geophys., 41, doi:10.1029/2002RG000121, 2003.

Crooks, S. A., and L. J. Gray: Characterization of the 11-year solar signal using a multiple regression analysis of the ERA-40 dataset, J. Climate, 18, 996-1015, 2005.

Fadnavis, S., and G. Beig: Decadal solar effects on temperature and ozone in the tropical stratosphere, Ann. Geophys., 24, 2091-2103, 2006a.

Fadnavis, S., and G. Beig: Seasonal variation of trend in temperature and ozone over the tropical stratosphere in the northern hemisphere, J. Atmos. Solar Terr. Phys., ?, doi:10.1016/j.jastp.2006.09.003, 2006b.

Fleming, E. L., S. Chandra, J. J. Barnett, and M. Corney: Zonal mean temperature, pressure, zonal wind and geopotential height as functions of latitude, Adv. Space Res., 10, (12)11-12(59), 1990.

Garcia, R. R., S. Solomon, R. G. Roble, and D. W. Rusch: A numerical response of the middle atmosphere to the 11-year solar cycle, Planet. Space Sci., 32, 411-423, 1984.

Gordley, L. L., M. E. Hervig, B. Magill, E. Thompson, M. McHugh, E. Remsberg, and J. Russell III: Accuracy of atmospheric trends inferred from HALOE data, for submission to J. Geophys. Res.-Atmos., 2006.

Grudzev, A. N., and G. P. Brasseur: Long-term changes in the mesosphere calculated by a two-dimensional model, J. Geophys. Res., 110, doi:10.1029/2003JD004410, 2005.

Hampson, J., P. Keckhut, A. Hauchecorne, and M. L. Chanin: The effect of the 11-year solar-cycle on the temperature in the upper-stratosphere and mesosphere—Part III: Investigations of zonal asymmetry, J. Atmos. Solar Terr. Phys., doi:10.1016/j.jastp.2006.05.006, 2006.

Hampson, J., P. Keckhut, A. Hauchecorne, and M. L. Chanin: The effect of the 11-year solar-cycle on the temperature in the upper-stratosphere and mesosphere—Part II, Numerical simulations and the role of planetary waves, J. Atmos. Solar Terr. Phys., doi:10.1016/j.jastp.2005.03.005, 2005.

Huang, T. Y. W., and G. P. Brasseur: Effect of long-term solar variability in a two-dimensional interactive model of the middle atmosphere, J. Geophys. Res., 98, 20,413-20,427, 1993.

Huang, F. T., H. G. Mayr, C. A. Reber, J. M. Russell, M. Mlynczak, and J. G. Mengel: Stratospheric and mesospheric temperature variations for the quasi-biennial and semiannual (QBO and SAO) oscillations based on measurements from SABER (TIMED) and MLS (UARS), Ann. Geophys., 24, 2131-2149, 2006.

Keckhut, P., C. Cagnazzo, M.-L. Chanin, C. Claud, and A. Hauchecorne: The 11-year solar-cycle effects on the temperature in the upper-stratosphere and mesosphere: Part I—Assessment of observations, J. Atmos. Solar Terr. Phys., doi:10.1016/j.jastp.2005.01.008, 2005.

Khosravi, R., G. Brasseur, A. Smith, D. Rusch, S. Walters, S. Chabrillat, and G. Kockarts: Response of the mesosphere to human-induced perturbations and solar variability calculated by a 2-D model, J. Geophys. Res., 107, doi:10.1029/2001JD001235, 2002.

Kirkwood, S., and K. Stebel: Influence of planetary waves on noctilucent cloud occurrence over NW Europe, J. Geophys. Res., 108, doi:10.1029/2002JD002356, 2003.

Kodera, K., and Y. Kuroda: Dynamical response to the solar cycle, J. Geophys. Res., 107, doi:10.1029/2002JD002224, 2002.

Kubicki, A., P. Keckhut, M-L Chanin, A. Hauchecorne, E. Lysenko, and G. S. Golitsyn: Temperature trends in the middle atmosphere as seen by historical Russian rocket launches: Part 1, Volgograd (48.68N, 44.35E), J. Atmos. Solar Terr. Phys., doi:10.1016/j.jastp.2006.02.001, 2006.

Laštovička, J., R. A. Akmaev, G. Beig, J. Bremer, J. T. Emmert: Global change in the upper atmosphere, Science, 314, 1253-1254, 2006.

Leblanc, T., I. S. McDermid, P. Keckhut, A. Hauchecorne, C-Y. She, and D. A. Kreuger: Temperature climatology of the middle atmosphere from long-term lidar measurements at middle and low latitudes, J. Geophys. Res., 104, 17,191-17,204, 1998.

Matthes, K., U. Langematz, L. L. Gray, K. Kodera, and K. Labitzke: Improved 11-solar signal in the Freie Universitat Berlin Climate Middle Atmosphere Model (FUB-CMAM), J. Geophys. Res., 109, D06101, doi:10.1029/2003JD004012, 2004.

Remsberg, E. E.: A re-analysis for the seasonal and longer-period cycles and the trends in middle atmosphere temperature from HALOE, J. Geophys. Res., in press, 2006.

Remsberg, E. E., and L. E. Deaver: Interannual, solar cycle, and trend terms in middle atmospheric temperature time series from HALOE, J. Geophys. Res., 110, D06106, doi:1029/2004JD004905, 2005.

Remsberg, E. E., P. P. Bhatt, and L. E. Deaver: Ozone changes in the lower stratosphere from the Halogen Occultation Experiment for 1991 through 1999, J. Geophys. Res., 106, 1639-1653, 2001.

Russell, J. M., III, L. L. Gordley, J. H. Park, et al.: The halogen occultation experiment, J. Geophys. Res., 98, 10,777-10,797, 1993.

Schmidt, H., G. P. Brasseur, M. Charron, et al.: The HAMMONIA chemistry climate model: sensitivity of the mesopause region to the 11-year solar cycle and CO_2 doubling, J. Climate, 19, 3903-3931, 2006.

Shepherd, M. G., G. G. Shepherd, W. F. J. Evans, and S. Sridharan: Global variability of mesospheric temperature: planetary-scale perturbations at equatorial and tropical latitudes, J. Geophys. Res., 110, doi:10.1029/2005JD006128, 2005.

Shepherd, M. G., W. F. J. Evans, G. Hernandez, D. Offermann, and H. Takahashi: Global variability of mesospheric temperature: mean temperature field, J. Geophys. Res., 109, doi:10.1029/2004JD005054, 2004.

Shindell, D., D. Rind, N. Balachandran, J. Lean, and P. Lonergan: Solar cycle variability, ozone, and climate, Science, 284, 305-308, 1999.

Shine, K. P., M. S., Bourqui, P. M. D. Forster, et al.: A comparison of model-simulated trends in stratospheric temperatures, Quart. J. Roy. Meteorol. Soc., 129, 1565-1588, 2003.

Table 1—Amplitudes and Phases of Terms at 3 and 5 hPa

P(hPa)	60S	50S	40S	30S	20S	10S	Eq	10N	20N	30N	40N	50N	60N
	AO Amplitude (K)												
3.0	19.9	17.2	11.4	6.6	2.5	0.5	1.1	1.0	1.7	3.6	7.4	12.0	17.4
5.0	19.4	16.1	9.0	4.1	1.5	0.4	0.7	0.8	1.5	2.8	7.0	11.0	14.7
	AO Phase (day of year of maximum)												
3.0	352	364	3	3	362	73	146	137	123	149	165	173	180
5.0	355	3	16	34	43	123	161	163	161	176	170	176	185
	SAO Amplitude (K)												
3.0	2.1	4.0	2.2	1.0	1.0	2.6	3.5	2.8	1.3	---	0.8	3.7	1.6
5.0	0.9	3.6	2.1	0.9	1.0	2.1	2.8	2.3	1.2	---	---	3.4	1.9
	SAO Phase (day of year for maximum of first cycle)												
3.0	42	48	73	71	110	120	118	119	118	---	52	20	24
5.0	46	61	86	90	119	131	127	128	126	---	---	23	28
	QBO Amplitude (K)												
3.0	0.8	1.2	1.2	0.6	0.5	0.8	1.1	0.7	0.5	1.2	1.5	1.1	---
5.0	1.0	1.2	1.1	0.5	---	0.5	1.0	0.6	0.4	0.8	1.2	0.9	---
	Annual Mean Term (K)												
3.0	247.5	246.0	246.8	249.3	250.8	251.5	251.8	251.8	251.2	250.5	249.1	247.9	245.1
5.0	238.3	236.8	237.4	239.8	241.3	242.1	242.5	242.3	241.7	240.9	239.6	238.2	236.4

Table 2—Adjusted, Max Minus Min, Values of SC-Like Terms (K)

P(hPa)	60S	50S	40S	30S	20S	10S	Eq	10N	20N	30N	40N	50N	60N
0.007	1.5	2.5	1.2	1.2	2.0	1.6	---	0.8	1.4	3.0	2.2	2.8	3.8
0.010	---	2.2	1.6	1.1	1.8	---	---	0.7	1.9	3.2	2.4	3.0	4.2
0.015	---	2.2	2.1	1.6	1.6	---	---	---	1.8	3.6	2.9	3.2	4.3
0.020	---	2.2	2.3	1.4	1.6	0.6	---	---	2.1	3.5	2.8	3.2	4.3
0.030	---	2.2	2.9	1.7	0.9	1.6	0.6	1.0	1.6	3.0	1.5	2.6	3.7
0.050	---	1.7	2.9	2.2	0.8	1.0	1.8	0.4	---	0.5	---	---	2.9
0.070	---	---	3.3	2.4	0.8	---	1.3	---	---	---	---	---	1.5
0.100	---	1.1	3.1	2.0	0.6	---	0.5	---	---	---	---	0.7	0.6
0.150	---	1.8	2.2	0.9	---	0.8	0.8	0.9	---	---	0.8	1.5	---
0.200	---	2.2	1.6	0.6	---	0.6	0.8	0.8	---	---	1.0	1.6	---
0.300	---	2.4	0.6	0.5	---	---	---	---	---	---	1.5	1.5	---
0.500	---	1.6	---	---	0.7	---	---	0.3	1.0	0.7	1.4	---	---
0.700	---	0.9	---	---	0.5	0.7	0.8	0.7	0.8	0.3	1.1	---	---
1.000	1.0	0.8	---	---	0.9	0.8	1.8	1.0	0.4	---	0.6	---	---
1.500	---	---	---	0.3	1.0	0.7	1.4	1.0	---	---	---	---	---
2.000	---	---	---	---	0.8	0.7	0.9	0.7	---	0.9	0.6	---	---

Table 3—SC-like, Max-Min, T(p) Response (K) by Latitude Zone

P(hPa)	50S-60S	20S-40S	10S-10N	20N-40N	50N-60N
0.007	2.0	1.5	1.2	2.2	3.3
0.010	2.2	1.5	0.7	2.5	3.6
0.015	2.2	1.8	0.7	2.8	3.7
0.020	2.2	1.8	0.6	2.8	3.7
0.030	2.2	1.8	1.1	2.0	3.1
0.050	1.7	2.0	1.1	0.5	2.9
0.070	1.4	2.2	1.3	0.7	1.5
0.100	1.1	1.9	0.5	0.7	0.6
0.150	1.8	1.5	0.8	0.8	1.5
0.200	2.2	1.1	0.7	1.0	1.6
0.300	2.4	0.6	0.5	1.5	1.5
0.500	1.6	0.7	0.3	1.0	---
0.700	0.9	0.5	0.7	0.7	---
1.000	0.9	0.9	1.2	0.5	---
1.500	---	0.7	1.0	0.6	---
2.000	---	0.8	0.8	0.7	---

Table 4—Linear Trend (K/decade) and Confidence Intervals (%)

P(hPa)	30S-40S		20S-20N		30N-40N	
0.007	---	---	-0.8	86	-0.6	86
0.010	---	---	-1.1	97	-0.5	65
0.015	-1.2	92	-1.2	86	-1.6	95
0.020	-2.1	98	-0.9	71	-2.3	99
0.030	-1.7	90	-0.8	75	-2.3	98
0.050	-1.9	96	-0.8	80	-1.8	90
0.070	-2.3	98	-1.3	96	-1.9	96
0.100	-2.4	99	-0.8	81	-1.6	94
0.150	-1.7	94	-1.0	98	-1.1	79
0.200	-1.3	73	-0.9	97	-0.8	79
0.300	-0.9	66	-0.5	89	-0.7	78
0.500	-0.7	65	-0.6	82	-0.6	78
0.700	-0.7	64	-0.8	93	-0.5	78
1.000	-0.6	63	-0.6	78	-0.5	75
1.500	-0.6	74	-0.6	84	-0.5	73
2.000	-0.8	97	-1.2	99	-1.3	93

Figure Captions

Figure 1—Time series of zonal average SR (open circles) and SS (solid circles) temperatures (K) from HALOE measurements at the Equator and the 0.15-hPa level of the mesosphere (near 62 km). Terms for the multiple linear regression (MLR) model fit are listed at the lower left. The oscillating curve is the fit for the complete MLR model, while the straight line is the value of the constant term.

Figure 2—As in Figure 1, but the SR and SS points have been adjusted by half the mean SR/SS difference and then refit with the MLR model.

Figure 3—Temperature residuals (K) for the MLR model fit to the data of Figure 2.

Figure 4—Contour plot of the zonal average temperature amplitude (K) for the semi-annual oscillation (SAO) term. Contour interval is 1 K. Altitude scale is approximate.

Figure 5—Phase (month of year) for the maximum of the first cycle of the SAO term.

Figure 6—As in Figure 4, but for the amplitude of the annual oscillation (AO) term. Contour interval is 2 K.

Figure 7—Phase (month of year) for the maximum of the AO term.

Figure 8—Contour plot of the annual-mean, zonal-average temperature distribution from the MLR model. Contour interval is 5 K.

Figure 9—Seasonal variation of the HALOE T(p) climatology for 20N. Contour interval is 5 K.

Figure 10—As in Figure 9, but for 40N.

Figure 11—As in Figure 4, but for the QBO term. Contour interval is 0.3 K.

Figure 12—As in Figure 4, but for the sub-biennial term. Contour interval is 0.3 K.

Figure 13—Average profiles of the adjusted, max minus min, differences of the T(p) response (K) for the 11-yr solar cycle (or SC-like) term of the MLR models for five separate latitude zones. The thick solid curve is for the 10S-10N zone.

Figure 14—Average profiles of the diagnosed, linear trend terms (in K/decade) for three separate latitude zones.

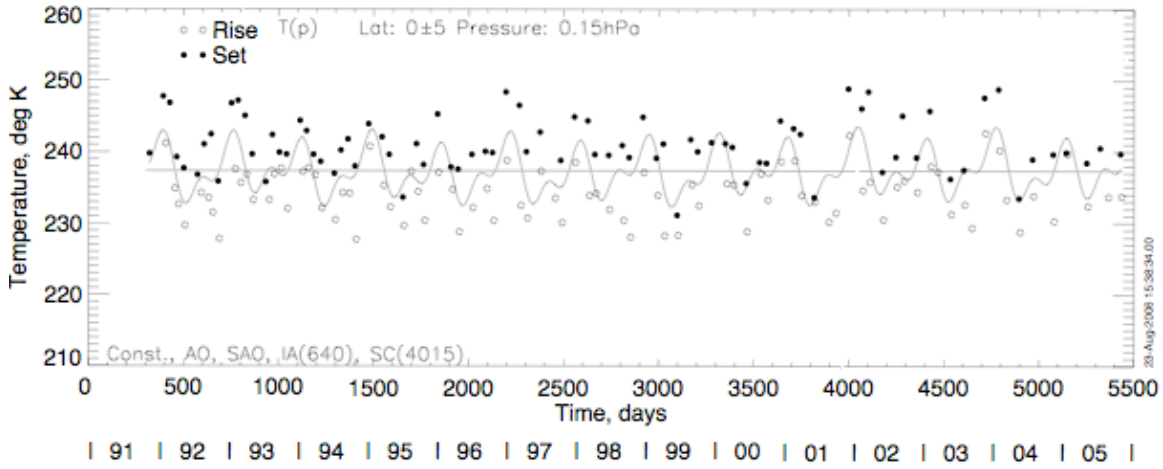
Rise
Set
T(p)
Lat: 0±5 Pressure: 0.15hPa
Temperature, deg K
260
250
240
230
220
210
Const., AO, SAO, IA(640), SC(4015)
0
500
1000
1500
2000
2500
3000
3500
4000
4500
5000
5500
Time, days
91
92
93
94
95
96
97
98
99
00
01
02
03
04
05

Fig.1

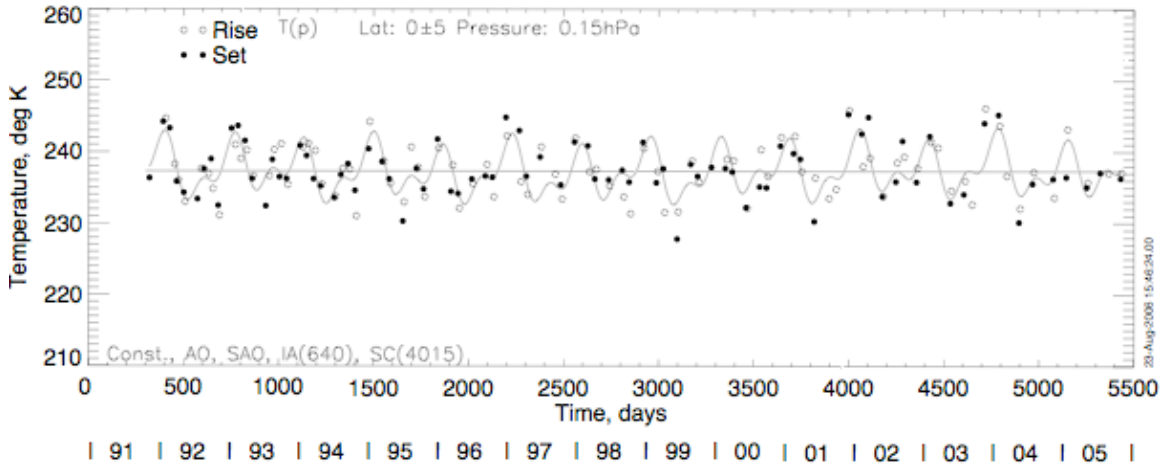
Rise
Set
T(p)
Lat: 0±5 Pressure: 0.15hPa
Temperature, deg K
260
250
240
230
220
210
Const., AO, SAO, IA(640), SC(4015)
0
500
1000
1500
2000
2500
3000
3500
4000
4500
5000
5500
Time, days
91
92
93
94
95
96
97
98
99
00
01
02
03
04
05

Fig.2

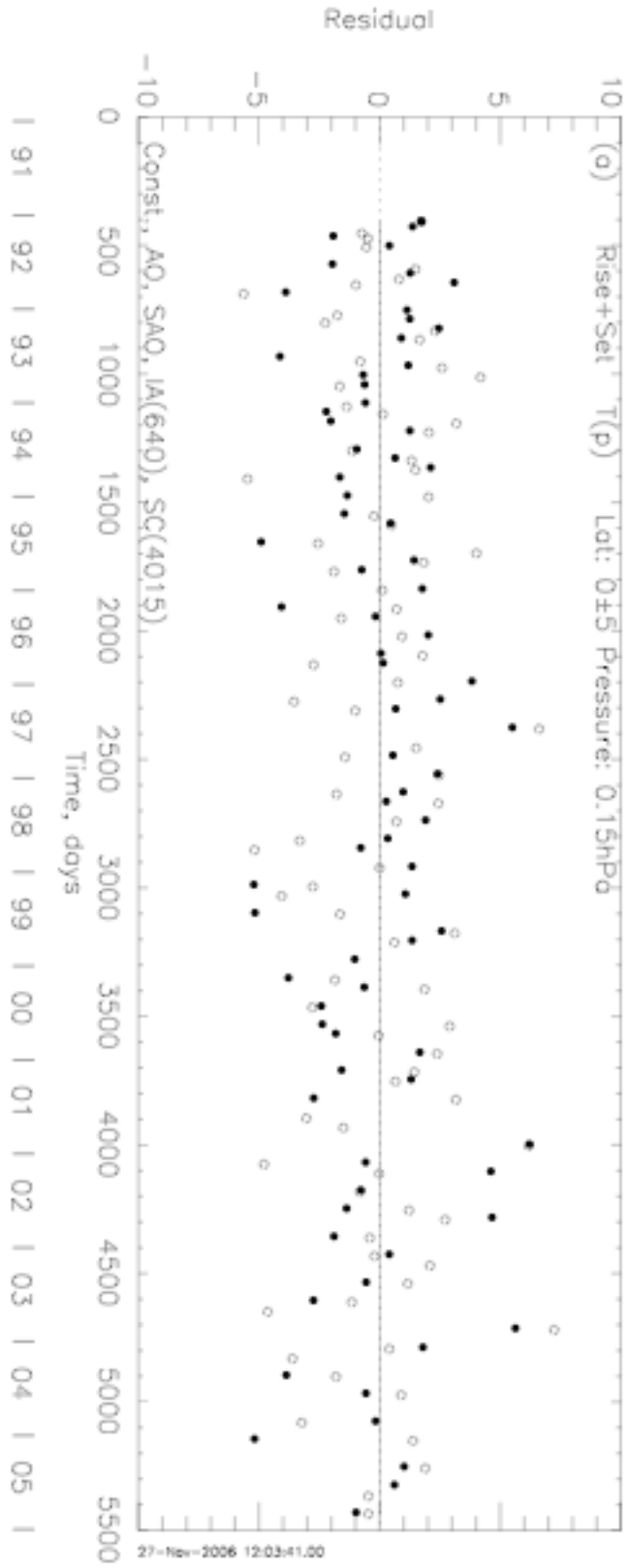
Residual
10
5
0
−5
−10
(a) Rise+Set T(p) Lat: 0±5 Pressure: 0.15hPa
Const., AO, SAO, IA(640), SC(4015)
0
500
1000
1500
2000
2500
3000
3500
4000
4500
5000
5500
Time, days
91
92
93
94
95
96
97
98
99
00
01
02
03
04
05
27-Nov-2006 12:03:41.00

Fig.3

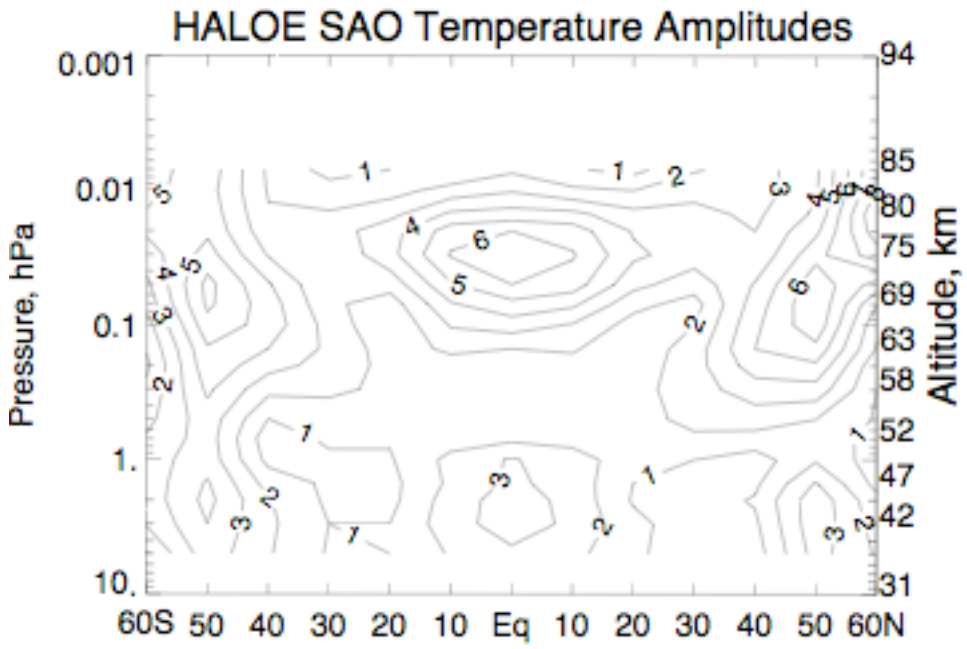
HALOE SAO Temperature Amplitudes
Pressure, hPa
0.001
0.01
0.1
1.
10.
Altitude, km
94
85
80
75
69
63
58
52
47
42
31
60S 50 40 30 20 10 Eq 10 20 30 40 50 60N

Fig.4

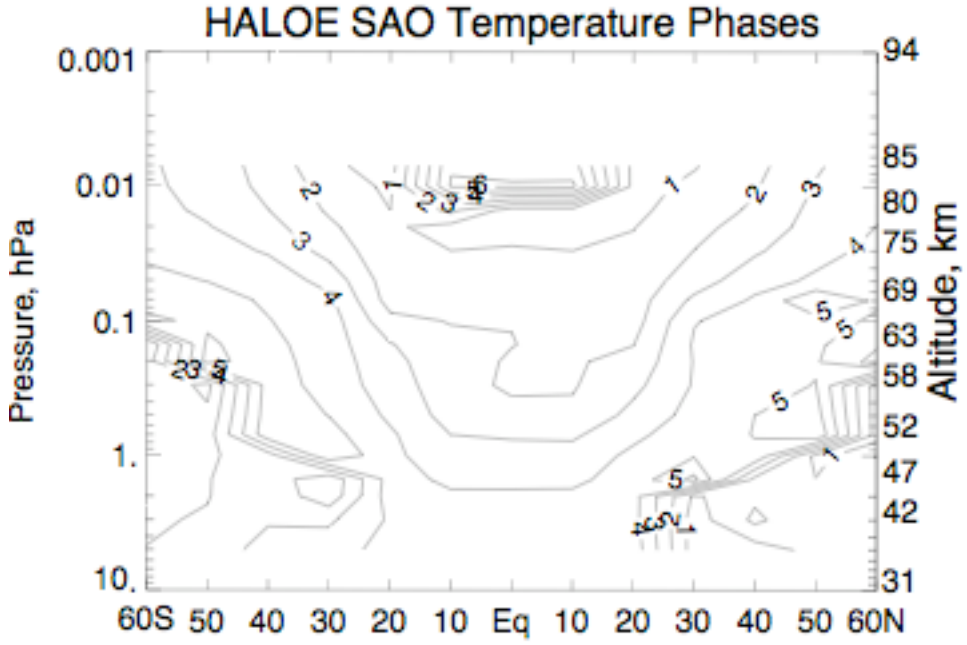
HALOE SAO Temperature Phases
Pressure, hPa
0.001
0.01
0.1
1.
10.
Altitude, km
94
85
80
75
69
63
58
52
47
42
31
60S 50 40 30 20 10 Eq 10 20 30 40 50 60N

Fig.5

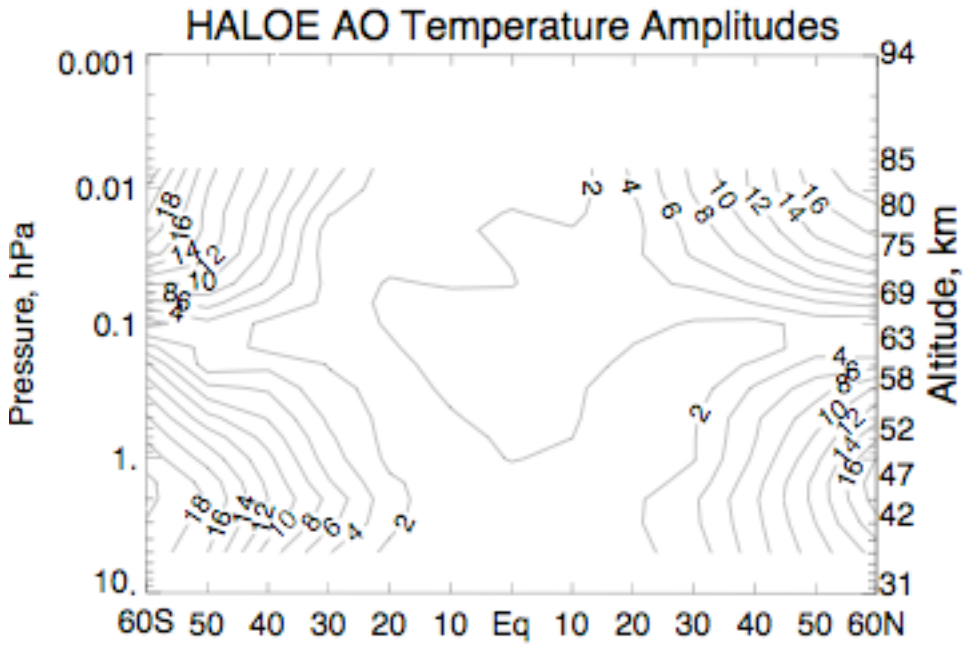
HALOE AO Temperature Amplitudes
Pressure, hPa
0.001
0.01
0.1
1.
10.
Altitude, km
94
85
80
75
69
63
58
52
47
42
31
60S 50 40 30 20 10 Eq 10 20 30 40 50 60N

Fig.6

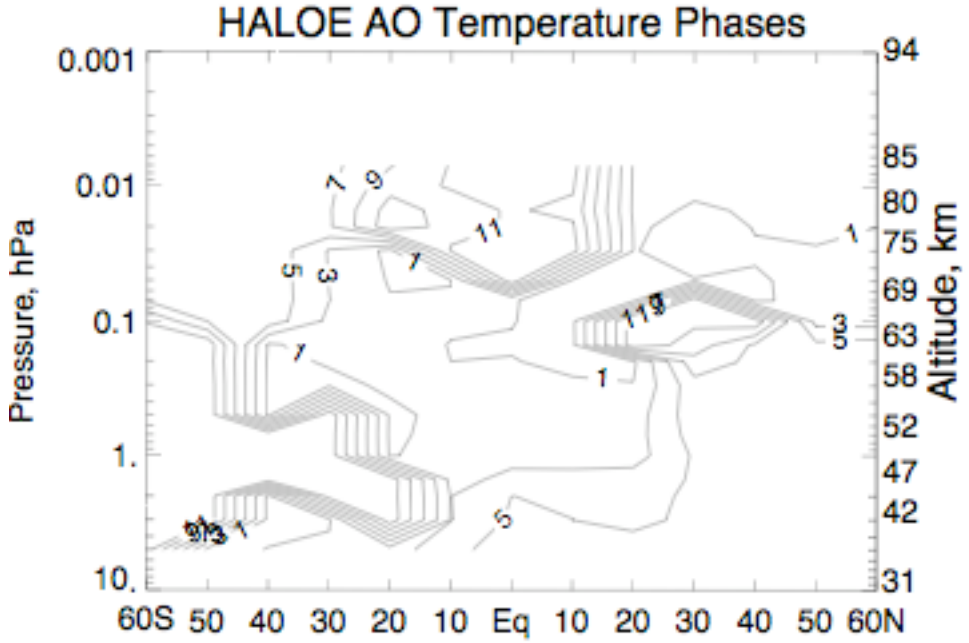
HALOE AO Temperature Phases
Pressure, hPa
0.001
0.01
0.1
1.
10.
Altitude, km
94
85
80
75
69
63
58
52
47
42
31
60S 50 40 30 20 10 Eq 10 20 30 40 50 60N

Fig.7

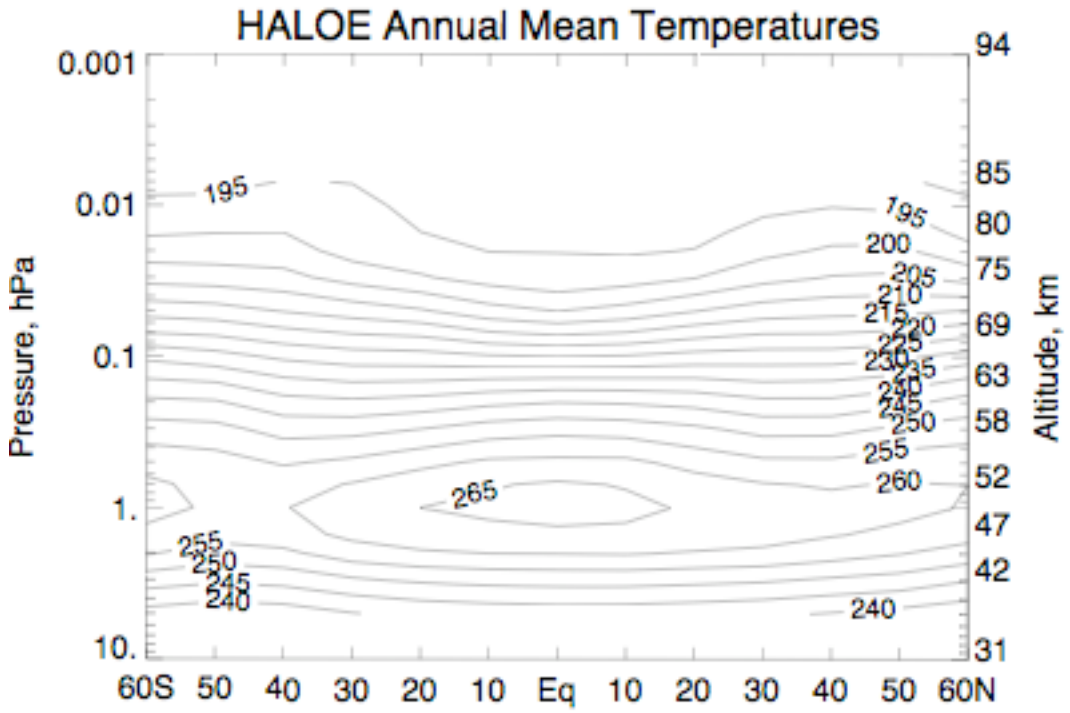
HALOE Annual Mean Temperatures
Pressure, hPa
Altitude, km
0.001
0.01
0.1
1.
10.
94
85
80
75
69
63
58
52
47
42
31
60S 50 40 30 20 10 Eq 10 20 30 40 50 60N
195
200
205
210
215
220
225
230
235
240
245
250
255
260
265

Fig.8

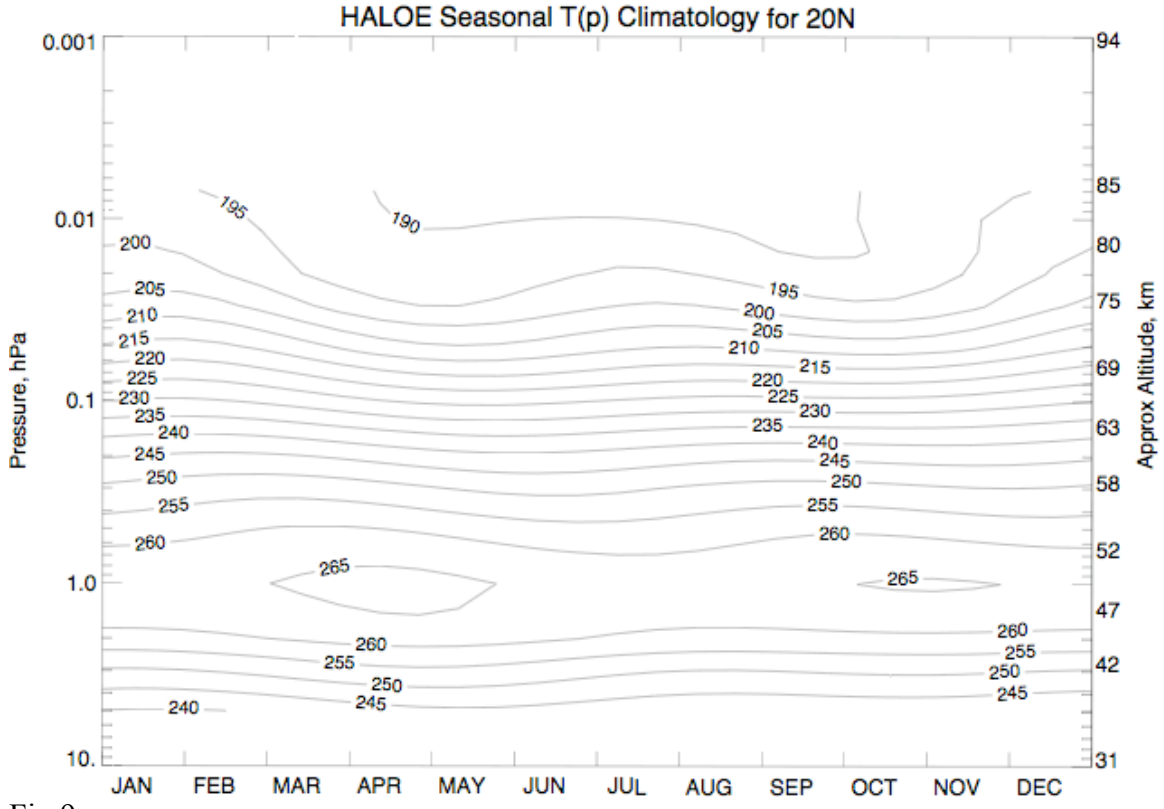
HALOE Seasonal T(p) Climatology for 20N
Pressure, hPa
Approx Altitude, km
0.001
0.01
0.1
1.0
10.
94
85
80
75
69
63
58
52
47
42
31
JAN FEB MAR APR MAY JUN JUL AUG SEP OCT NOV DEC
190
195
200
205
210
215
220
225
230
235
240
245
250
255
260
265

Fig.9

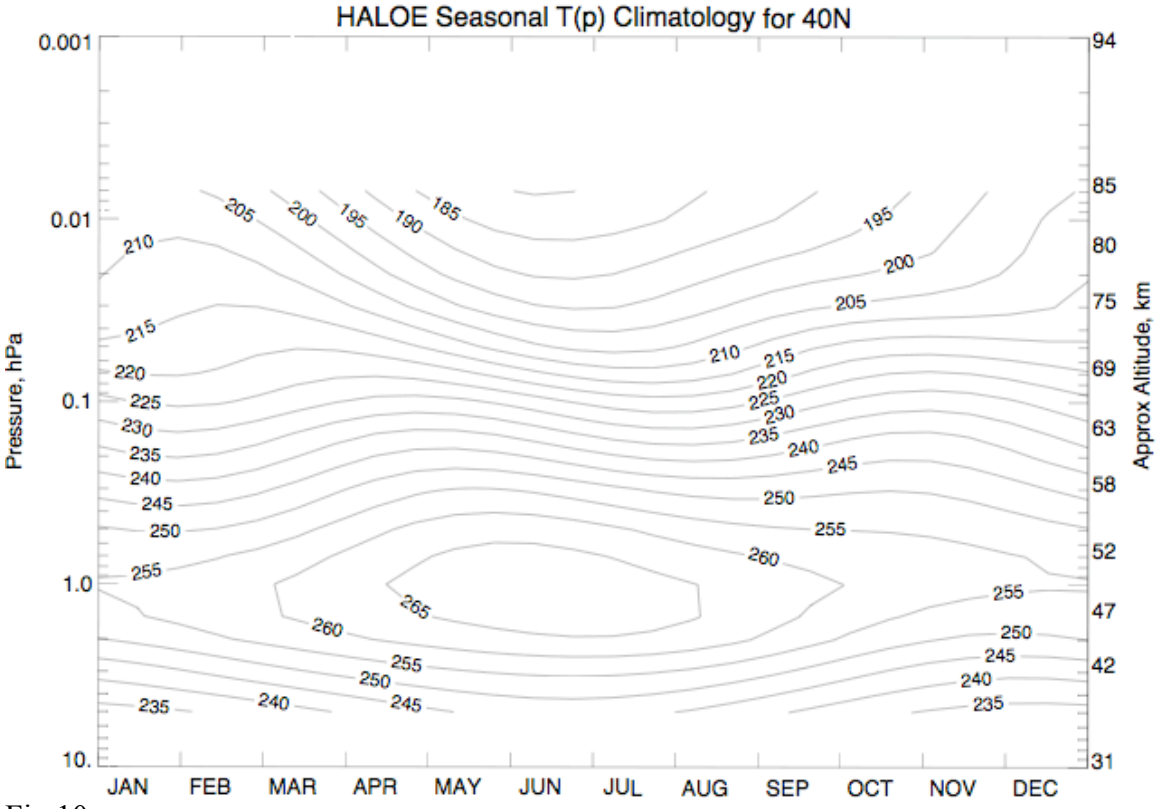
HALOE Seasonal T(p) Climatology for 40N
Pressure, hPa
Approx Altitude, km
0.001
0.01
0.1
1.0
10.
94
85
80
75
69
63
58
52
47
42
31
JAN
FEB
MAR
APR
MAY
JUN
JUL
AUG
SEP
OCT
NOV
DEC

Fig.10

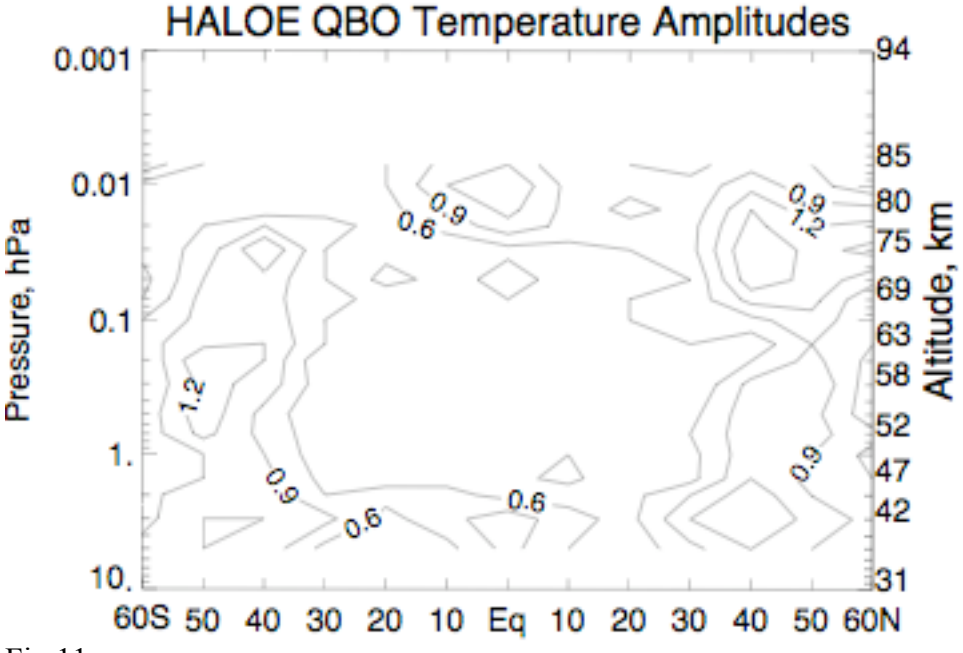
HALOE QBO Temperature Amplitudes
Pressure, hPa
Altitude, km
0.001
0.01
0.1
1.
10.
94
85
80
75
69
63
58
52
47
42
31
60S
50
40
30
20
10
Eq
10
20
30
40
50
60N

Fig.11

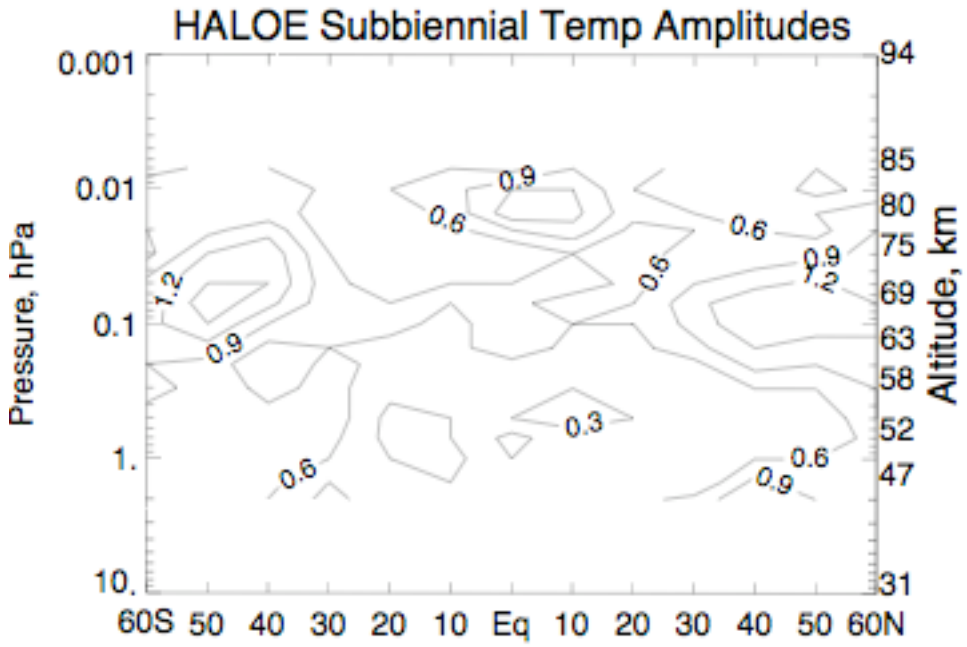
HALOE Subbiennial Temp Amplitudes
Pressure, hPa
0.001
0.01
0.1
1.
10.
Altitude, km
94
85
80
75
69
63
58
52
47
31
60S 50 40 30 20 10 Eq 10 20 30 40 50 60N
0.9
0.6
0.6
0.6
0.9
1.2
0.9
0.3
0.6
0.6
0.9
Fig.12

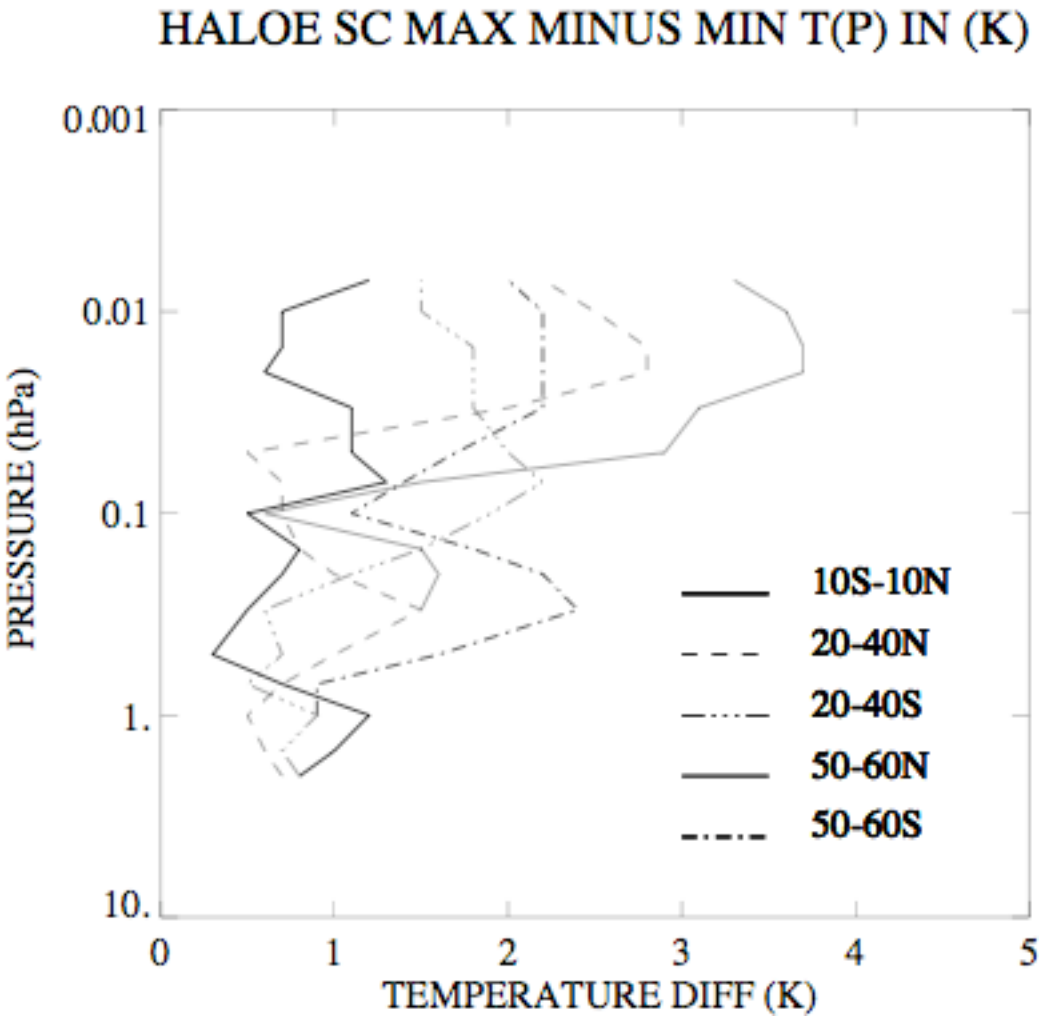
HALOE SC MAX MINUS MIN T(P) IN (K)
0.001
0.01
0.1
1.
10.
PRESSURE (hPa)
0
1
2
3
4
5
TEMPERATURE DIFF (K)
10S-10N
20-40N
20-40S
50-60N
50-60S

Fig.13

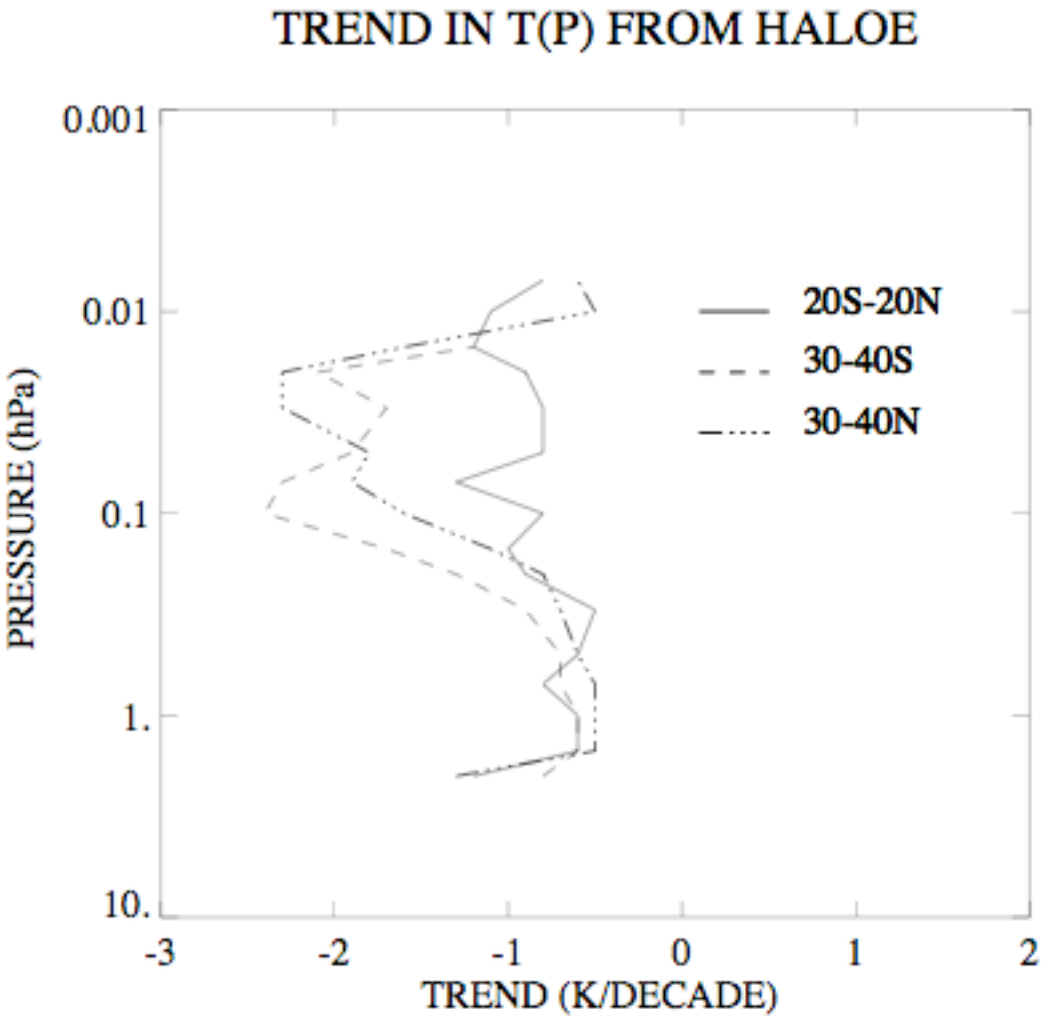
TREND IN T(P) FROM HALOE
0.001
0.01
0.1
1.
10.
PRESSURE (hPa)
-3
-2
-1
0
1
2
TREND (K/DECADE)
20S-20N
30-40S
30-40N

Fig.14